TÜBİTAK

Turkish Journal of Physics

http://journals.tubitak.gov.tr/physics/

Research Article

Turk J Phys
(2019) 43: 355 – 364

doi:10.3906/fiz-1812-13

# Ab initio study of $Li_2CaTa_2O_7$ compound: electronic and optical properties for three phases

**Murat AYCİBİN***
Department of Physics, Faculty of Science, Van Yüzüncü Yıl University, Van, Turkey

**Received:** 13.12.2018 • **Accepted/Published Online:** 02.07.2019 • **Final Version:** 02.08.2019

**Abstract:** The $Li_2CaTa_2O_7$ compound belongs to the Ruddlesden–Popper family of layered perovskites. First principle approximation was used to investigate the electronic band structure and optical properties of the compound for three phases. Independent of the studied compound's structural type, $Li_2CaTa_2O_7$ has semiconductor behavior and direct transition. In addition, the forbidden energy band gap of the compound decreases with rising temperature, as expected. Furthermore, the 3d orbital of Ca contributes to the conduction band due to the crystal field effect. Moreover, the optical response of the chosen axes of the compound to incoming electromagnetic rays varies with phase transition.

**Key words:** Electronic structure, lattice constant, density of states, Wien2K, Ruddlesden–Popper phase, $Li_2CaTa_2O_7$

## 1. Introduction

The crystal structure of layered perovskite type compounds has attracted countless researchers' attention due to their interesting properties such as ion exchange, ion conduction, $CO_2$ capture, ferroelectricity, and catalytic activity [1–5]. The forms of Dion–Jacobson (DJ), Ruddlesden–Popper (RP), and Aurivillius phases are counted as major families of closely related layered perovskite [1–6].

The $Li_2CaTa_2O_7$ (LCTO) compound belongs to the RP type layered perovskites and its detailed structural information was given in previous research [2,3]. There are limited experimental works and no theoretical studies related to LCTO. The first study on LCTO was performed by Liang et al. [3], who showed that LCTO has high photocatalytic properties and the structure of the compound was determined at room temperature. Eight years later, Berre et al. investigated LCTO. They used several techniques to characterize the compound and observed that the compound undergoes a structural phase transition, which is an important phenomenon for the emergence and evolution of a number of physical/chemical properties in solid-state materials [7]. Moreover, they gave structural information of LCTO for all structural phases [2]. Wang et al. measured the AC impedance of the $Li^+/H_2CaTa_2O_7$ compound and compared it with original LCTO [5]. Wiley et al. used microwave and solvothermal methods to investigate series of topochemical reactions. In their study, LCTO was one of the chosen samples [8]. Ramakrishnan et al. performed an experimental study to investigate ionic properties of three RP materials ($Li_2CaTa_2O_7$, $Li_2SrNb_2O_7$, and $Li_2CaTa_2O_7$) [9]. Furthermore, the crystal information of LCTO has also been given online [10,11].

Unfortunately, there is a lack of experimental and theoretical information related to the electronic and optical properties of this compound for all phases. In this paper, I report a theoretical study devoted to the

*Correspondence: murataycibin@yyu.edu.tr

$Li_2CaTa_2O_7$ compound to calculate the electronic band structure and optical properties with the Wien2k [12] program for three phases. This will be a very useful guide for researchers who will study the LCTO compound.

## 2. Computational methods

To extract ground state information for the electronic structure and related properties of the compound, an ab initio method was applied. The ground state electronic properties were calculated using the linearized augmented plane wave (LAPW) [8] implemented in density functional theory (DFT), which is the best tool for researchers to calculate electronic properties of solids due to the well-established scheme.

For calculation purposes, the following parameters were used for Wien2K software: –9 Ry energy separation between valance and core bands was chosen for cut-off energy. In the Brillion zone (BZ), 98 high symmetry k points in an 11 × 11 × 3 grid was selected for the density, potential, and wave function. To calculate physical properties of compounds, an approximate exchange-correlation energy was required by practical application of DFT. There are four different potentials embedded in Wien2K, namely the local spin density approximation (LSDA) [13], the Perdew–Burke–Ernzerhof [14] , WC-GGA [15,16], and PBEsol-GGA [17].

## 3. Results and discussion

### 3.1. Structural properties

The LCTO compound undergoes a structural phase transition from $Pna2_1$ to Pnma and Pnma to Cmcm with temperature change [2]. Structural information of LCTO for three structural cases was given by Berre et al. [2]. In that study, they gave the space group, lattice parameters, and atomic positions for three cases. The atomic electronic configuration of the compound is Li [He] $2s^1$, Ca [Ar] $4s^2$, Ta [Xe] $4f^{14}$ $5d^3$ $6s^2$, and O [He] $2s^2$ $2p^4$.

The first task is to determine which potential embedded in the Wien2K software will be used for exchange-correlation effects. Therefore, volume optimization was run to obtain the best theoretical lattice parameter closest to the experimental value at room temperature (Figure 1). In the optimization progress, the total energy of the unit cell for each potential is calculated by varying unit cell volume and plotted versus corresponding energy. Afterwards, the Birch–Murnaghan equation of state [18] was used to extract theoretical values of the lattice constant. The obtained theoretical lattice constants depending on selected potential are given in Table 1.

**Table 1**. Calculated ground state lattice constants of LCTO depending on chosen pseudopotential at room temperature.

| Lattice constant (Å) | PBE-GGA | LSDA | WC-GGA | PBEsol-GGA | Experimental [2] |
|---|---|---|---|---|---|
| **a** | 5.652 | 5.477 | 5.459 | 5.481 | 5.514471 |
| **b** | 5.603 | 5.430 | 5.412 | 5.434 | 5.466341 |
| **c** | 18.695 | 18.117 | 18.057 | 18.130 | 18.2393 |

It is clear from Table 1 that the calculated lattice constants closest to the experimental values were obtained by applying PBEsol-GGA potential. To be consistent, PBEsol-GGA potential has been used for the rest of the calculations during the calculation of physical properties of LCTO for all structural types. Figure 2 shows pressure versus volume. From Figure 2, it is seen that energy in a more stable condition corresponding to minimum volume was obtained at zero pressure.

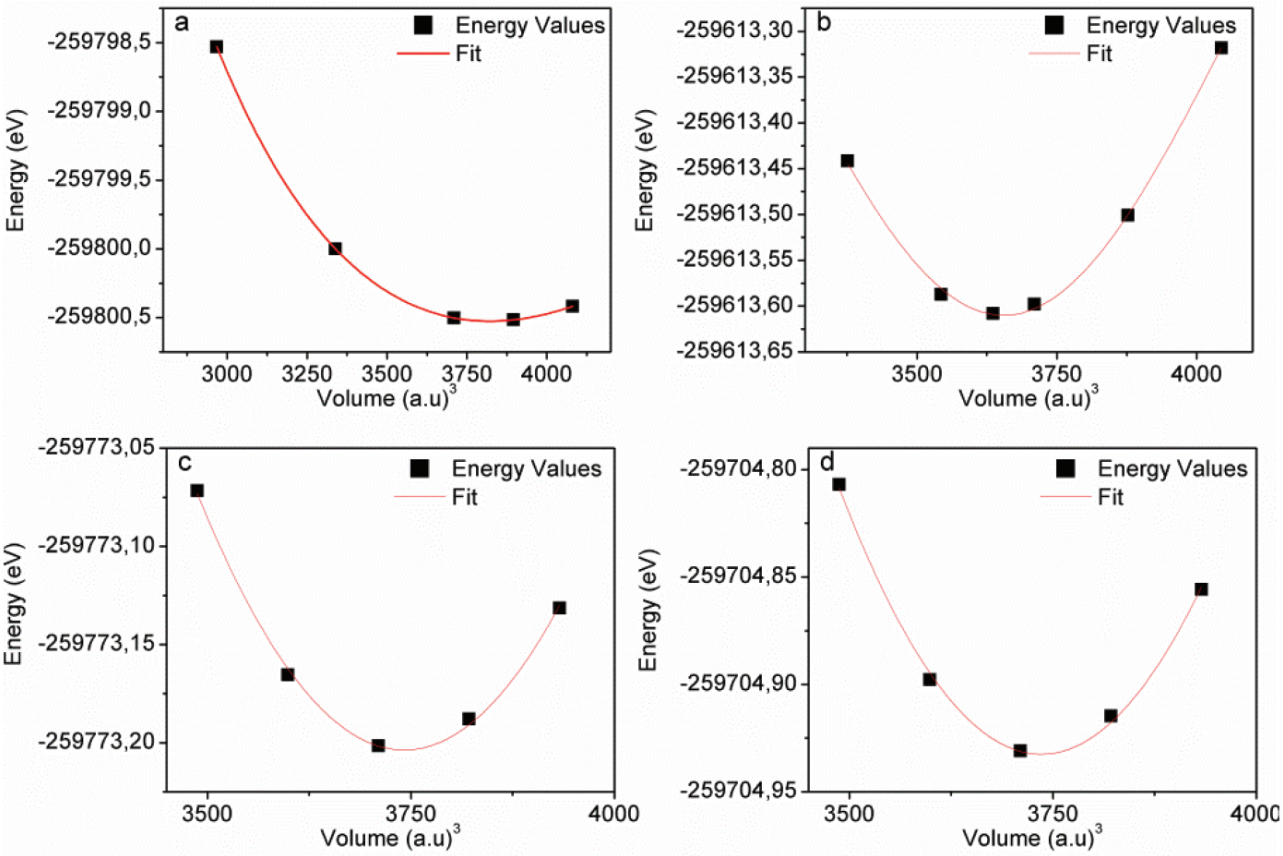


**Figure 1**. Total energy versus unit cell volume by chosen potential: a) PBE-GGA, b) LSDA, c) PBEsol-GGA, and d) WC-GGA for LCTO at room temperature.

### 3.2. Electronic properties

After determination the potential energy, the electronic band structure of the LCTO compound for each phase was obtained with Wien2K software (Figure 3). In Figure 3, the Fermi energy level is set to origin. Also, the forbidden energy band gap (FEBG) values for every case are obtained as a 2.635 eV, 2.540 eV, and 2.297 eV. It is clear that the FEBG value of the compound gets smaller due to rising temperature and phase transition. In addition, LCTO is classified as a semiconductor with a wide band gap value for all cases. Furthermore, both the top of the valence band (red line) and the bottom of the conduction band (green line) are located at the Γ high symmetry point in the BZ, which implies direct transition.

To use semiconductor materials as voltaic cell material, the FEBG should be in the range of 1 eV to 4 eV. According to the obtained results, regardless of the studied case, the FEBG of LCTO makes the compound a good candidate for voltaic cell applications.

The electronic density of states (DOS) and the atom-resolved partial density of states (PDOS) of LCTO at zero pressure are also shown in Figure 4. The first outstanding feature observed is the large energy band gap between the conduction band and valance band. This energy band gap also confirms that the compound is a semiconductor with a large band gap value. To see phase transition effects on the FEBG value in DOS, Figure 5 was drawn. It is easily seen that the starting point of the conduction band shifts to a small energy value with a structural phase transition (small window in Figure 5).

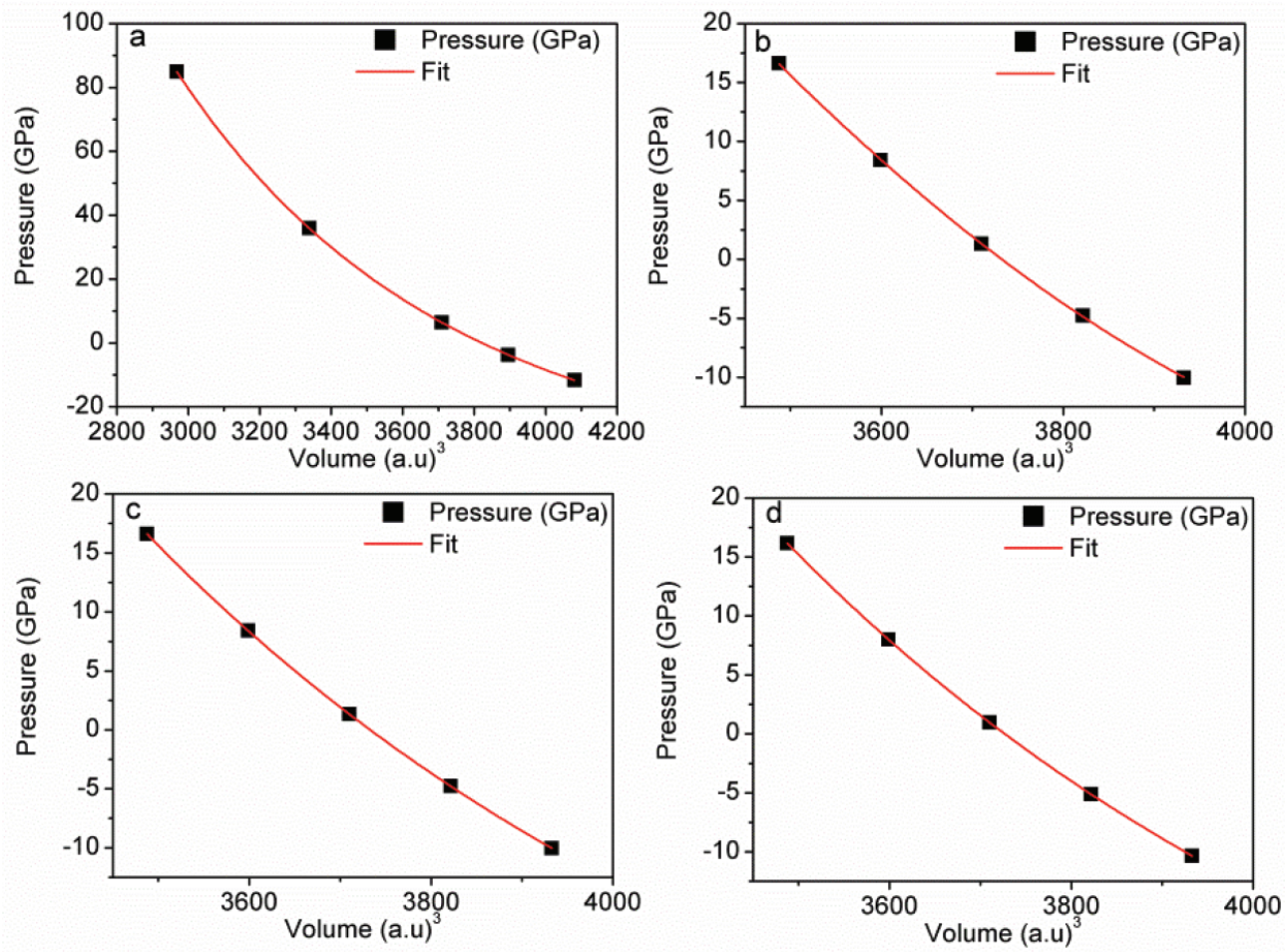


**Figure 2**. Pressure versus unit cell volume by chosen potential: a) PBE-GGA, b) LSDA, c) PBEsol-GGA, and d) WC-GGA for LCTO at room temperature.

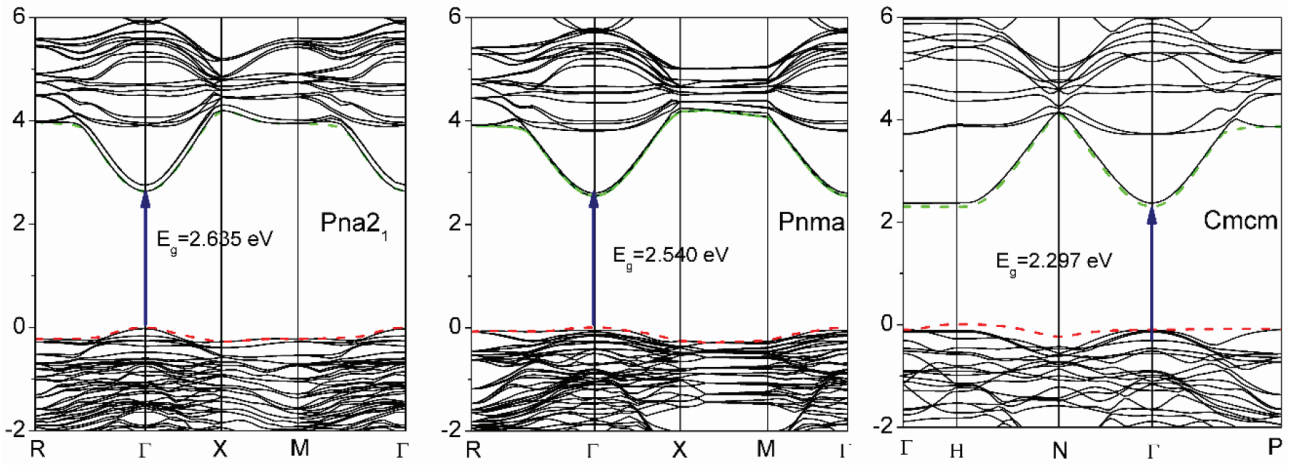


**Figure 3**. Calculated electronic band structure of LCTO for three temperature values.

The partial contribution of atoms also was calculated by Wien2K and plotted (Figure 4). Regardless of the studied phase, while the Ca atom contributes the conduction band, the valence band of the compound was

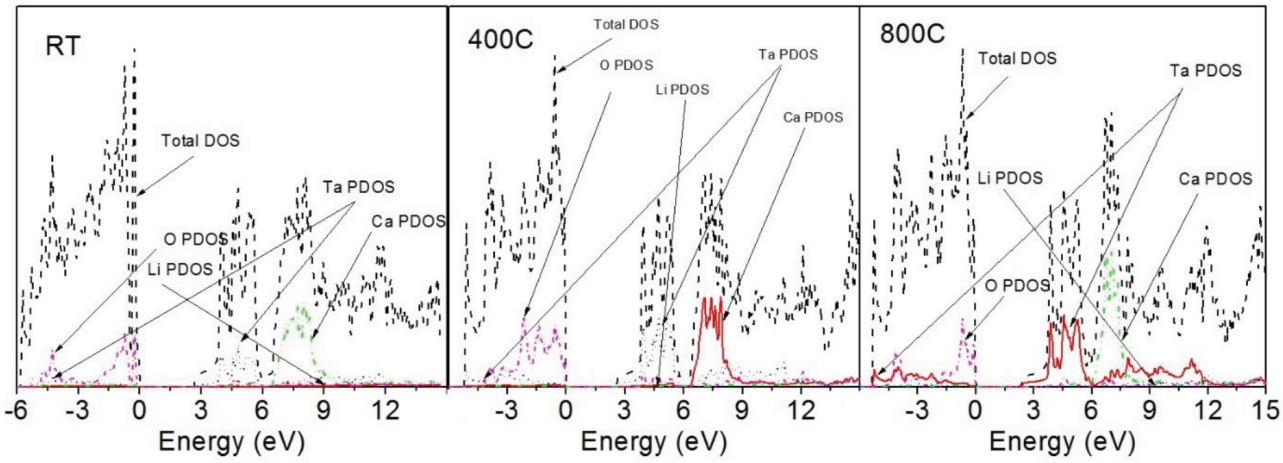


**Figure 4**. Calculated TDOS of LCTO compound for three different temperature values.

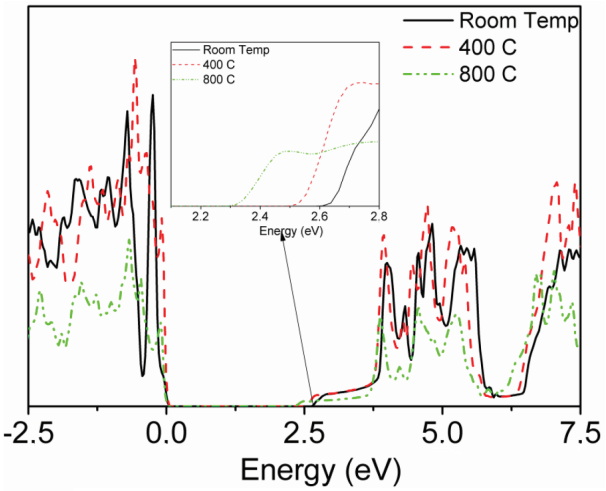


**Figure 5**. The effect of temperature on FBGE in TDOS of LCTO.

mainly formed by the O atom. In addition, tantalum contributes to not only the valence band but also the conduction band. Moreover, the contribution of the Li atom is almost negligible compared with other atoms' contributions. The partial contribution of the Ca atom also needs to be addressed here (Figure 6). It is well known that the electronic configuration of the Ca atom ends up with $4s^2$. However, the d orbital of the Ca atom has contributed to the conduction band (Figure 6), which implies a transition from the s orbital to d orbital such as that due to crystal field effect.

### 3.3. Optical properties

In this section, the optical responses of the compound for different phases are analyzed and discussed. The dielectric equation, $\varepsilon(\omega) = \varepsilon^1(\omega) + \varepsilon^2(\omega)$, describes the linear response of a system to an external electromagnetic field. While $\varepsilon^1(\omega)$ represents the real part of the dielectric function, $\varepsilon^2(\omega)$ is known as the imaginary part and $\omega$ is the light frequency.

The type of material structure plays an important role in calculating the dielectric function. If the studied compound has an orthorhombic structure, all diagonal components of the dielectric tensor depending on the

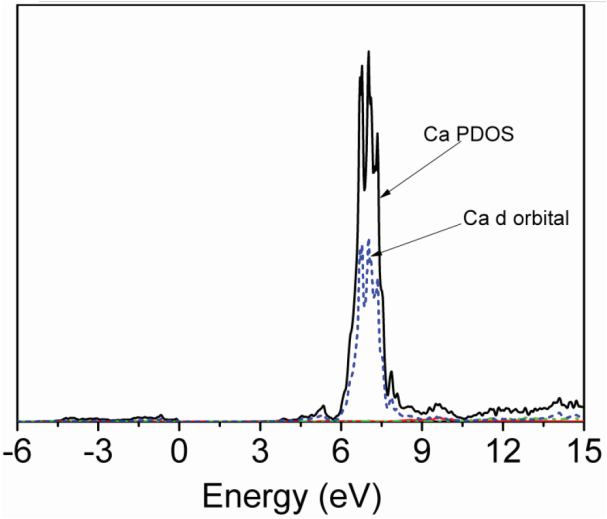


**Figure 6**. The partial contribution of Ca atom to DOS.

calculated axes have to be calculated. LCTO crystal has an anisotropic orthorhombic structure; therefore, we calculated all axes-dependent components of dielectric function (Figure 7).

Knowledge of the dielectric function of the compound gives us an opportunity to understand the electronic structure of compound. All dielectric components were calculated within the 0–42 eV or 0–50 eV photon energy range. The chosen energy range is sufficient to calculate and determine the values of optical components of LCTO. The incident radiation with linear polarization was only considered during the calculation process.

Like the forbidden band gap, the static value of the dielectric constant, $\varepsilon(0)$, is a very important physical quantity for semiconductors. The static values of the real part of the dielectric constant of all cases were obtained (small windows in Figure 7) and are given in Table 2. It is obvious from Table 2 that while the value of $\varepsilon_x^1(0)$ gets larger with the phase transition, the value of $\varepsilon_z^1(0)$ gets smaller. In addition, $\varepsilon_y^1(0)$ first has higher value and then it gets smaller. That is normal due to phase transition with temperature change, and the response to incoming incident light also changes. Detailed analysis of Figure 7 reveals that the real part of the dielectric constant for different phases has negative values between 9.075 and 12.20 eV, 26.81 and 27.90 eV, and 39.19 and 39.57 eV. In these regions, the compound behaves like metal and reflects all incident electromagnetic light back to the incoming direction. Finally, $\varepsilon_x^1(\omega)$ belonging to the Pna21 space group at room temperature has the lowest value at 9.075–12.20. When the temperature rises to 400 °C, the compound undergoes the first structural phase transition and $\varepsilon_y^1(\omega)$ has the lowest value. Moreover, $\varepsilon_z^1(\omega)$ has the lowest value at 800 °C, where the second phase transition, Pnma to Cmcm, takes place. The component change of the real part with the structural phase transition implies that the crystal direction response to the incident electromagnetic light is altered.

**Table 2**. Calculated static values of real part of dielectric function of LCTO.

| | Room temperature | 400 °C | 800 °C |
|---|---|---|---|
| $\varepsilon_{1xx}(0)$ | 4.59 | 4.69 | 4.78 |
| $\varepsilon_{1yy}(0)$ | 4.71 | 4.82 | 4.72 |
| $\varepsilon_{1zz}(0)$ | 4.74 | 4.72 | 4.71 |

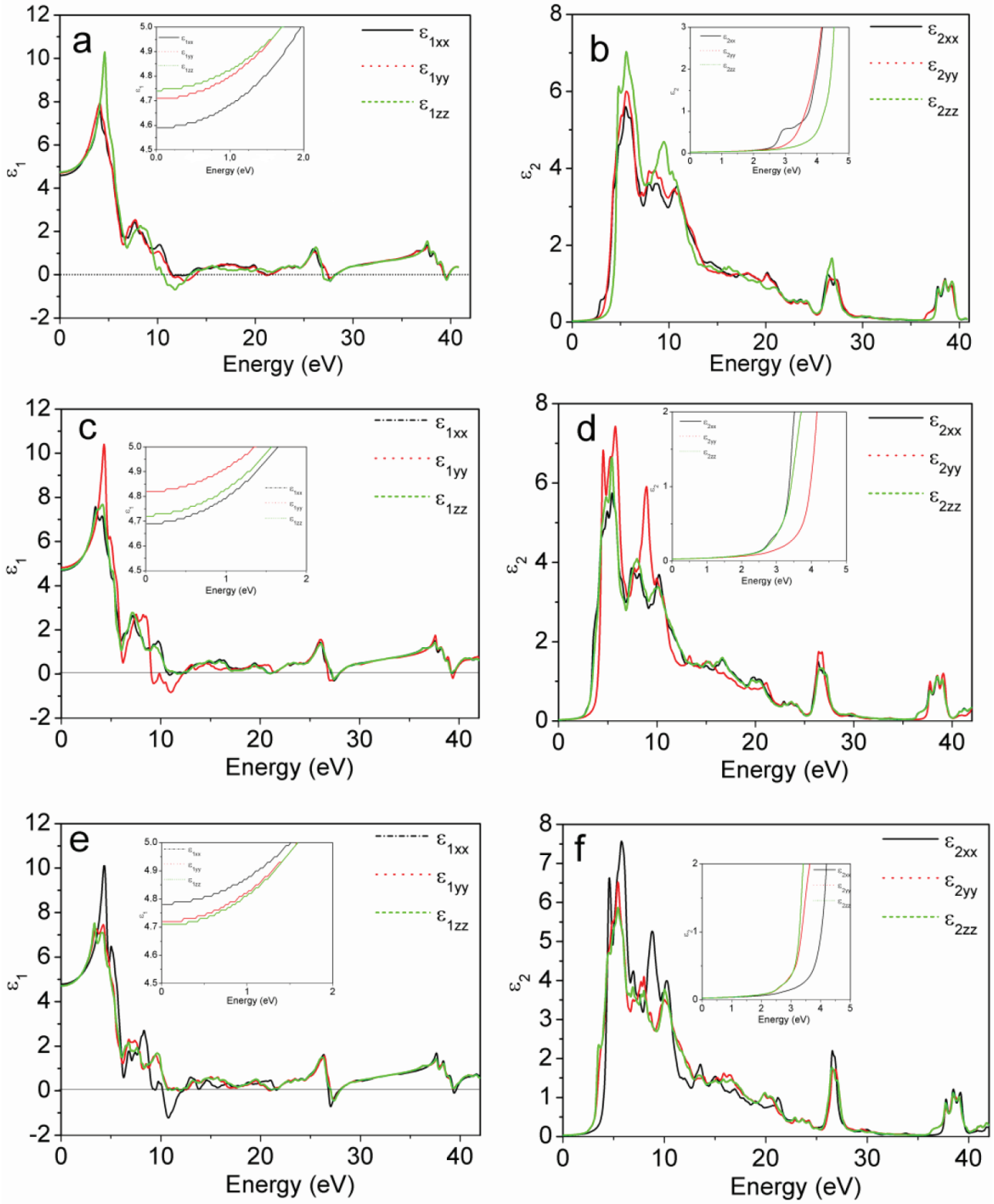


**Figure 7**. Real, $\varepsilon_1(\omega)$, and imaginary, $\varepsilon_2(\omega)$, parts of dielectric function of LCTO compound axes dependence: a, b) room temperature; c, d) 400 °C; e, f) 800 °C.

The imaginary part of the dielectric function is directly related to resistivity, which means dissipation of energy. There is a dramatic increase (small windows in Figure 7) after 2.62, 2.46, and 2.27 eV corresponding to the energy band gap for $Pna2_1$, Pnma, and Cmcm phases, respectively. The maximum peak of the imaginary part of the dielectric constant located between 5.78 and 5.79 eV is responsible for strong optical transitions independent of temperature.

Figure 8 shows the refractive index through the crystal axes for all phases. The refractive index defines how the light propagates through the material. Obtained static values of the refractive index depending on the axis are given in Table 3. It is seen from Table 3 and Figure 8 that the refractive index value of the selected axes varies because of structural phase transition. Moreover, it is also known that when the FEBG gets smaller, the refractive index has a larger value. The characteristic correlation between the forbidden band gap and refractive index is also observed (Table 3).

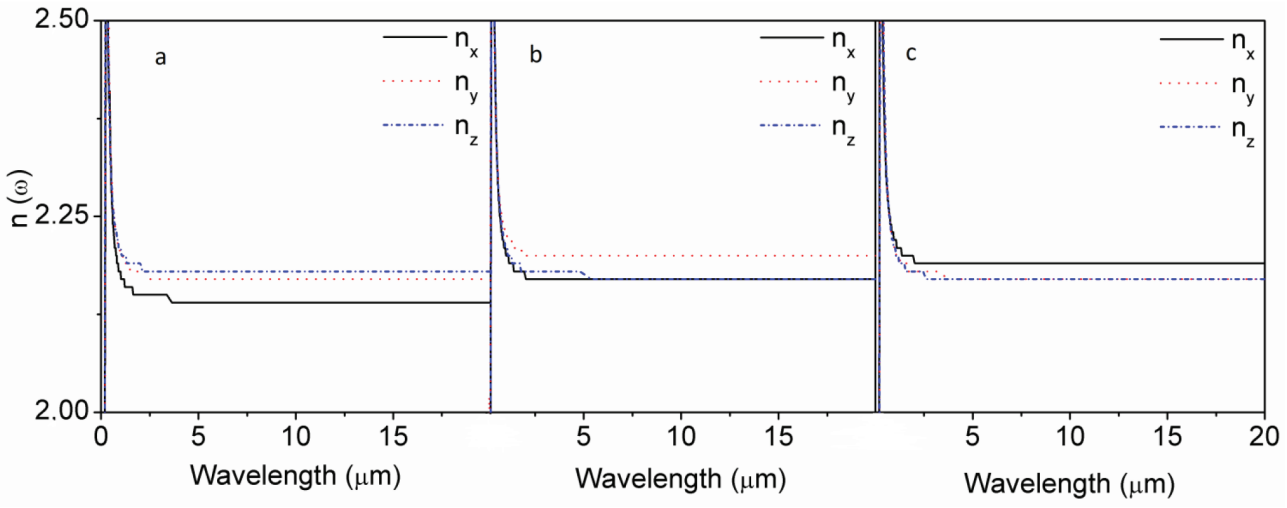


**Figure 8**. Temperature dependence of the refraction coefficient of the LCTO compound along x, y, and z axes: a) room temperature, b) 400 °C, c) 800 °C.

**Table 3**. Calculated temperature dependence of the static values of refractive index of LCTO.

| | Room Temperature | 400 °C | 800 °C |
|---|---|---|---|
| $n_{xx}(0)$ | 2.14 | 2.17 | 2.19 |
| $n_{yy}(0)$ | 2.17 | 2.20 | 2.17 |
| $n_{zz}(0)$ | 2.18 | 2.17 | 2.17 |

Finally, reflectivity versus energy is plotted in Figure 9. With detailed analysis of Figure 9, it is seen that the maximum reflection, 40%, occurs at 40 eV for the $Pna2_1$ phase, while it ensues at 29 eV for not only Pnma but also the Cmcm phase. In addition, more light is reflected back by the z-axis for $Pna2_1$, by the x-axis for Pnma, and by the y-axis for Cmcm phases. Due to structural changes, this is an expected situation. In addition, the maximum 40% of the incident electromagnetic wave is reflected back and 60% of incoming light goes through the material for all phases. One more detail is that all incident light goes through materials at 26 eV and between 35 and 38 eV energy values.

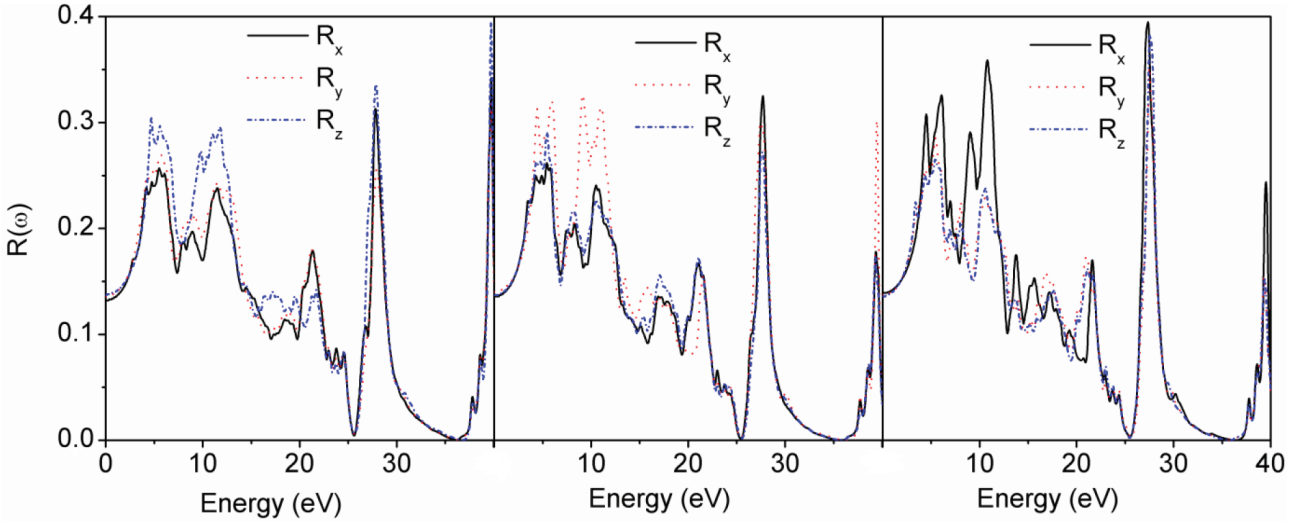


**Figure 9**. Temperature dependence of the reflection coefficient of LCTO compound along x, y, and z axes: a) room temperature, b) 400 °C, c) 800 °C.

## 4. Conclusion

In this study, some physical properties of the $Li_2CaTa_2O_7$ compound for all phases were investigated and analyzed. Regardless of temperature changes, the forbidden energy band gap lies in the energy range of 2.2–2.7 eV, where the compound has semiconductor behavior with direct transition. The forbidden energy value makes the compound a good candidate for voltaic cell applications in technological areas.

The real and imaginary parts of the dielectric function were calculated and interpreted according to the studied axis. The value of the static real part of the dielectric function is in the range of 4.59–4.71 eV depending on the axis. The compound has reflected back a maximum of 40% of the incident electromagnetic wave regardless of temperature. In addition, the refractive index depending on the axis was calculated.

Unfortunately, there are few experimental studies in the literature. Researchers have investigated structural properties of the compound such as lattice parameters, atomic position, phase transition depending on temperature, and ionic properties. There is no information about the electronic, structure, and optical properties of the compound obtained from either experimental study or theoretical performance. Therefore, the calculated data were not compared.

## Acknowledgment

This work was supported by the Scientific Research Projects Unit of Yüzüncü Yıl University under Project No. 2015-FED-YL348.

## References

[1] Armstrong AR, Anderson PA. Synthesis and structure of a new layered niobium blue bronze - $Rb_2LaNb_2O_7$. Inorganic Chemistry 1994; 33 (19): 4366-4369. doi: 10.1021/ic00097a026

[2] Galven G, Mounier D, Bouchevreau B, Suard E, Bulou A et al. Phase transitions in the Ruddlesden-Popper phase Li2CaTa2O7:X-ray and neutron powder thermodiffraction, TEM, Raman, and SHG experiments. Inorganic Chemistry 2016; 7; 55 (5): 2309-23. doi: 10.1021/acs.inorgchem.5b02659

[3] Liang ZH, Tang K, Shao Q, Li G, Zeng S et al. Synthesis, crystal structure, and photocatalytic activity of a new two-layer Ruddlesden-Popper phase, $Li_2CaTa_2O_7$. Journal of Solid State Chemistry 2008; 181 (4): 964-970. doi: 10.1016/j.jssc.2008.01.042

[4] Toda K, Takahashi K, Teranishi T, Ye ZG, Sato M et al. Synthesis and structure determination of reduced tantalates, $Li_2LaTa_2O_7$, $Li_2Ca_2Ta_3O_{10}$ and $Na_2Ca_2Ta_3O_{10}$, with a layered perovskite structure. Journal of Materials Chemistry 1999; 9 (3): 799-803. doi: 10.1039/a807038E

[5] Wang Y, Hao Q, Li X, Li B, Luo J et al. Preparation of a $Li^+$ intercalated organic derivative of the Ruddlesden-Popper phase $H_2CaTa_2O_7$. Journal of Alloys and Compounds 2015; 645: 24-28. doi: 10.1016/j.jallcom.2015.05.011

[6] Gopalakrishnan J, Bhat V, Raveau B. $A^ILaNb_2O_7$ : A new series of layered perovskites exhibiting ion-exchange and intercalation behavior. Materials Research Bulletin 1987; 22 (3): 413-417. doi: 10.1016/0025-5408(87)90060-2

[7] Fujimoto M. The Physics of Structural Phase Transitions. 2nd ed. Berlin, Germany: Springer, 2005.

[8] Akbarian-Tefaghi S, Vegia ET, Amnad G, Wiley JB. Rapid topochemical modification of layered perovskites via microwave reactions. Inorganic Chemistry 2016; 55 (4): 1604-1612. doi: 10.1021/acs.inorgchem.5b02514

[9] Ramakrishnan P, Kwak H, Cho Y, Kim JH. Ionic conductivity of Ruddlesden-Popper layered perovskites ($Li_2SrTa_2O_7$, $Li_2SrNb_2O_7$, and $Li_2CaTa_2O_7$) with poly (ethylene oxide) as a composite solid electrolyte. ChemElectroChem 2018; 5: 1265-1271. doi: 10.1002/celc.201800017

[10] Jain A, Ong SP, Hautier G, Chan W, Richards WD et al. Commentary: The Materials Projects: A materials genome approach to accelerating materials innopvation. APL Materials 2013; 1 (1): 011002. doi: 10.1063/1.4812323

[11] Villars P, Cenzual E (editors). $Li_2CaTa_2O_7$ Crystal Structure: Datasheet from "PAULING FILE Multinaries Edition – 2012". Berlin, Germany: SpringerMaterials, 2012 (https://materials.springer.com/isp/crystallographic/docs/sd_1220953).

[12] Blaha P, Schwarz K, Madsen GKH, Kvasnicka D, Luitz J et al. *WIEN2k*, An Augmented Plane Wave + Local Orbitals Program for Calculating Crystal Properties. Vienna, Austria: Technical University of Vienna, 2018.

[13] Perdew JP, Wang Y. Accurate and simple analytic representation of the electron-gas correlation-energy. Physical Review B 1992; 45 (23): 13244-13249. doi: 10.1103/PhysRevB.45.13244

[14] Perdew JP, Burke K, Ernzerhof M. Generalized gradient approximation made simple. Physical Review Letters 1996; 77 (18): 3865-3868. doi: 10.1103/PhysRevLett.77.3865

[15] Wu ZG, Cohen RE. More accurate generalized gradient approximation for solids. Physical Review B 2006; 73 (23): 235116 . doi: 10.1103/PhysRevB.73.235116

[16] Wu ZG, Cohen RE. Comment on "More accurate generalized gradient approximation for solids". Physical Review B 2008; 78 (19): 197101. doi: 10.1103/PhysRevB.78.197101

[17] Perdew JP, Ruzsinszky A, Csonka GI, Vydrov OA, Scuseria GE et al. Restoring the density-gradient expansion for exchange in solids and surfaces. Physical Review Letters 2008; 100 (13): 136406. doi: 10.1103/PhysRevLett.100.136406

[18] Birch F. Finite elastic strain of cubic crystals. Physical Review 1947; 71 (11): 809-824. doi: 10.1103/PhysRev.71.809

[19] Murnaghan FD. The compressibility of media under extreme pressures. Proceedings of the National Academy of Sciences of the United States of America 1944; 30 (9): 244-247. doi: 10.1073/pnas.30.9.244